

Waveform Proportionality and Taylor's Law Induced by Synchronization of Periodic and Chaotic Oscillators

Yuzuru Mitsui* and Hiroshi Kori†

Graduate School of Frontier Sciences, The University of Tokyo

(Dated: November 27, 2023)

Taylor's law (TL), the scaling relationship between the mean and variance, has been observed in various fields. However, the underlying reasons why TL is so widely observed, why the exponents of TL are often close to 2, and the relationship between temporal and spatial TLs are not fully understood. Here, using coupled oscillator models, we analytically and numerically demonstrate that synchronization can induce TL. In particular, we show that strong synchronization leads to waveform proportionality, resulting in temporal and spatial TLs with exponent 2. Our study can help infer the existence of synchronization solely from the relationship between the mean and variance.

Introduction. Taylor's law [1, 2] (TL) is a power law relationship between the mean and variance:

$$\log(\text{variance}) = \log \alpha + \beta \times \log(\text{mean}). \quad (1)$$

TL has been observed in various fields, such as population ecology [2], biophysics [3], and complex networks [4–6], among others [7, 8]. TL is also known as fluctuation scaling in physics [7]. Especially, when $\beta > 1$, the relationship Eq. (1) is sometimes called giant number fluctuations. It has been investigated experimentally [9] and theoretically [10–12], and attracts significant attention in the field of active matter [13–16]. TL has been extensively analyzed via theoretical studies [3, 17–34], and it is usually classified into two types, i.e., temporal TL and spatial TL. In temporal TL, the means and variances are computed from data recorded at multiple time points at a given place, whereas in spatial TL, the means and variances are computed from data recorded at multiple places at a given time point.

Various studies have attempted to clarify the mechanisms of TL. Although theories show that TL exponent β can take any real values [25–27], exponents close to 2 have been often observed in real data in ecosystems for both temporal and spatial TLs [24, 28, 35]. Cohen and Xu showed that when multiple independent random variables follow the same distribution, a correlation appears between the mean and variance by random sampling if the distribution is skewed [20]. While their results shed light on the ubiquity of TL, the reason for the observed TL exponents in ecosystems being often close to 2 remained unclear because TL exponents can take arbitrary values depending on the shape of distribution. By applying large deviations theory and finite-sample arguments, Giometto et al. showed that, depending on the sampling method, exponent 2 may be frequently observed in spatial TL [19]. Reuman et al. showed that correlations between random variables affect the exponent of spatial TL [18]. In particular, spatial TL with exponent 2 is observed when there exists a proportional relationship between time series [18]. As a mechanism for the emergence of TL with exponents close to 2, the correlation between time series is considered crucial, and synchronization is

strongly implicated as the mechanism that generates such correlations. Moreover, studies employing numerical simulations of dynamical systems have shown that synchronization affects both temporal and spatial TL exponents [28, 30, 31]. It is noteworthy that when the degree of correlation between time series increases, exponents of temporal and spatial TLs approach 2 [22, 24, 36].

In this study, we showed that in a broad class of dynamical system models, including ecosystem models, synchronization generates a special correlation, which we call waveform proportionality, between time series, resulting in temporal and spatial TLs with exponent 2.

Model and results. First, we define TL for a given time-series set $x_i(t)$ ($i = 1, \dots, N$). For temporal TL, we compute the mean and variance of each site i as $E[x_i(t)]_t = \langle x_i(t) \rangle_t$ and $V[x_i(t)]_t = \langle (x_i(t) - E[x_i(t)]_t)^2 \rangle_t$, respectively, where $\langle \cdot \rangle_t$ denotes the long-time average or average over 1 cycle when $x_i(t)$ is periodic in t . A linear fitting to N data points of $(\log E[x_i(t)]_t, \log V[x_i(t)]_t)$ yields slope β_t and intercept $\log \alpha_t$. For spatial TL, the mean and variance at time t are expressed by $E[x_i(t)]_i = \langle x_i(t) \rangle_i$ and $V[x_i(t)]_i = \langle (x_i(t) - E[x_i(t)]_i)^2 \rangle_i$, respectively, where $\langle \cdot \rangle_i$ denotes the average over site i . A linear fitting to M data points of $(\log E[x_i(t)]_i, \log V[x_i(t)]_i)$, where M is the number of sample times, yields slope β_s and intercept $\log \alpha_s$. In either case, R^2 denotes the coefficient of determination for linear fitting.

Our results are based on the model describing a population of oscillators, where oscillator i ($i = 1, \dots, N$) obeys:

$$\dot{x}_i = f_x(x_i, y_i, z_i) + D_x(X - x_i), \quad (2a)$$

$$\dot{y}_i = f_y(x_i, y_i, z_i) + D_y(Y - y_i), \quad (2b)$$

$$\dot{z}_i = f_z(x_i, y_i, z_i) + D_z(Z - z_i). \quad (2c)$$

We consider a food chain model with global coupling as our first example. Concretely, we consider $f_x = a(x_i - x^*) - lx_i y_i$, $f_y = -b_i(y_i - y^*) + lx_i y_i - ky_i z_i$, $f_z = -c(z_i - z^*) + ky_i z_i$, $X = \langle x_i \rangle_i$, $Y = \langle y_i \rangle_i$, and $Z = \langle z_i \rangle_i$, where x_i , y_i , and z_i denote the populations of the vege-

tation, herbivores, and predators at site i , respectively; $\langle w_i \rangle_i = \frac{1}{N} \sum_{i=1}^N w_i$ is the average of population w_i ($w_i = x_i, y_i, z_i$) over site i ; and $a, b_i, c, l, k, x^*, y^*$, and z^* are parameters describing intrinsic dynamical properties [37–39]. Heterogeneity across sites can be expressed by parameter b_i in accordance with [37–39]. The second terms in Eq. (2) describe diffusive coupling with strength D_x, D_y , and D_z . We assume that inhomogeneity can be denoted by parameter $b_i = b_0 + \mu_i$, where b_0 is the mean $\langle b_i \rangle_i$ and μ_i is the deviation from the mean. Note that $\langle \mu_i \rangle_i = 0$; specifically, μ_i is selected from a uniform distribution between -0.1 and 0.1 , and sorted in ascending order. For convenience, we introduced a reference oscillator, $i = 0$, that obeys Eq. (2) with $b_i = b_0$ and $D_x = D_y = D_z = 0$. This model demonstrates synchronized oscillations for a wide range of parameters when the coupling strength is comparable or larger than $\max|\mu_i|$. The upper panels of Fig. 1 illustrate the typical waveforms of $x_i(t)$. As evident in Figs. 1 (b)-(d), the oscillators are synchronized in frequency in the presence of sufficiently strong coupling.

Next, we verify temporal and spatial TLs in Fig. 2, where the blue symbols represent the mean-variance relations. TL with exponent close to 2 is observed when D_y is sufficiently large. Moreover, temporal TL becomes evident for $D_y = 0.8$, whereas spatial TL seems to require stronger coupling. To determine the underlying mechanism of TL, we carefully observed the waveforms shown in the upper panel of Fig. 1(d), which yielded well-defined temporal and spatial TLs. All waveforms were found to be considerably similar. Moreover, they were approximately proportional to $x_0(t)$ (data not shown). Thus, we hypothesized that the following relation approximately holds true for all i and t :

$$x_i(t) = C_i x_0(t), \quad (3)$$

where C_i is constant; this relation is hereafter referred to as the *waveform proportionality*. Under such a relation, both temporal and spatial TLs are evidently valid with exponent $\beta_{t,s} = 2$, as shown below. First, note that $E[x_i(t)]_t = C_i E[x_0(t)]_t$, $V[x_i(t)]_t = C_i^2 V[x_0(t)]_t$, $E[x_i(t)]_i = E[C_i] x_0(t)$, and $V[x_i(t)]_i = V[C_i] (x_0(t))^2$. By eliminating C_i and $x_0(t)$ from these relations, we obtain the following temporal and spatial TLs:

$$V[x_i(t)]_t = \alpha_t E[x_i(t)]_t^{\beta_t}, \quad (4)$$

$$V[x_i(t)]_i = \alpha_s E[x_i(t)]_i^{\beta_s}, \quad (5)$$

where

$$\alpha_t = \frac{V[x_0(t)]_t}{E[x_0(t)]_t^2}, \quad (6a)$$

$$\alpha_s = \frac{V[C_i]_i}{E[C_i]_i^2}. \quad (6b)$$

Here, $\beta_t = \beta_s = 2$. To verify this hypothesis, we plot the ratio $\zeta_i(t) = \frac{x_i(t)}{x_j(t)}$, where j is a reference oscillator, as

shown in the bottom panels of Fig. 1. The choice of j may be arbitrary; however, here, we selected $j = N/2 = 50$ because $x_{N/2}$ is expected to be close to x_0 . It is now clear that waveform proportionality approximately arises in the waveforms in Fig. 1(d) but not in those in other panels. This suggests that waveform proportionality spontaneously emerges in strongly synchronized oscillators. TL with exponent $\beta_{t,s} = 2$ then naturally occurs.

Next, we quantitatively investigate the dependence of the synchronization level and TL exponent on the coupling strength, D_y (Fig. 3). Here, the order parameter χ for synchronization can be defined as

$$\chi = \frac{CV[X(t)]}{\max_i \{CV[x_i(t)]\}}, \quad (7)$$

where CV represents the coefficient of variation. Namely, χ is the coefficient of variation of the mean-field of $x_i(t)$ normalized by the maximum coefficient of variation of $x_i(t)$. This quantity is close to 1 when the oscillators are completely synchronized; it is close to 0 when the oscillators are desynchronized. The same χ is plotted in Figs. 3(a) and (c). Moreover, $\log \alpha_{t,s}$ is illustrated in Fig. S1. Depending on the value of D_y , quenching may occur, rendering it impossible to define χ . Thus, we judged that quenching occurred when the mean of the variance of $x_i(t)$, $1/N \sum_{i=1}^N \langle (x_i(t) - \langle x_i(t) \rangle_t)^2 \rangle_t$, was less than a certain threshold value, and such cases were excluded. The number of times we judged that quenching occurred is shown in Fig. S2. We confirmed that qualitatively same results could be obtained for several different threshold values. This process was applied to all systems described later.

It can be observed in Figs. 3(a) and (b) that β_t approached a value close to 2 as D_y increased. Around $D_y \approx 0.5$, R^2 was sufficiently close to 1 and β_t was close to 2. Thus, temporal TL with exponent $\beta_t \approx 2$ was observed around $D_y = 0.5$. In contrast, according to χ , synchronization began at approximately $D_y = 0.05$, significantly earlier than the onset of temporal TL. These results suggest that in addition to synchronization, there exists an unidentified condition responsible for the emergence of temporal TL. The onset of spatial TL was significantly slower than that of temporal TL. To identify the cause of this phenomenon, we focused on the waveform of $D_y = 0.8$, where only temporal TL was observed (Figs. 2(c) and (g)). Here, waveform proportionality was not realized well (Fig. 1(c), bottom); however, when the waveforms were shifted such that their peak positions coincided, the ratio $\zeta_i(t)$ became almost constant, as shown in Fig. S3(c). This indicates that the hypothesis considered in Eq. (3) should be replaced with $x_i(t) = C_i x_0(t - t_i)$. We further found the shift t_i to be approximately proportional to μ_i and $1/D_y$ (Figs. S4 and S5). These results suggest that waveform proportionality occurs with a lag t_i , which decreases when D_y

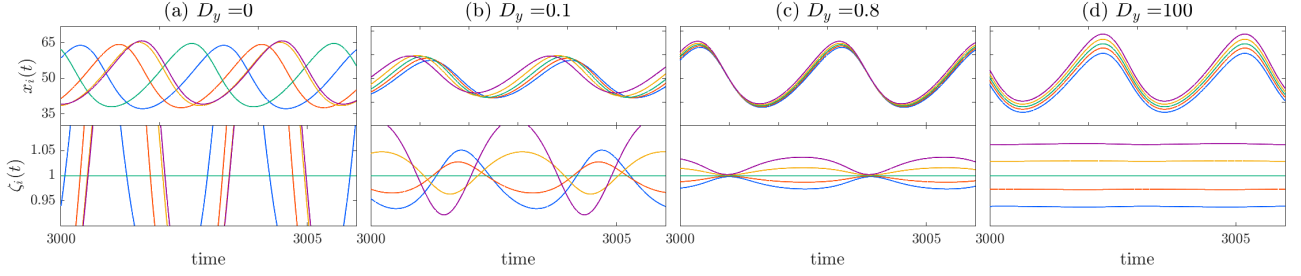


FIG. 1. Examples of $x_i(t)$ and $\zeta_i(t)$ for each coupling strength. Upper and lower panels show the time series and ratio of time series, respectively. $N = 100, D_x = 0, D_z = 0, a = 1, c = 9, k = 0.6, l = 0.1, x^* = 1.6, y^* = 0,$ and $z^* = 0.01$. b_i was randomly selected from a uniform distribution between 4.9 and 5.1. Data for $i = 1, 25, 50, 75,$ and 100 are shown.

is increased. Because Eq. (4) holds true even when $x_i(t) = C_i x_0(t)$ is replaced with $x_i(t) = C_i x_0(t - t_i)$, temporal TL emerges at smaller D_y . In contrast, Eq. (5) is violated in the presence of lag; thus, spatial TL may appear only when the lag is vanishingly small, i.e., D_y is considerably large. Accordingly, we found that spatial TL is observed for a wider range of D_y upon using shifted waveforms $x_i(t + t_i)$, as shown in red symbols in Figs. 2(g) and (h), and Fig. S6.

To theoretically clarify the mechanism responsible for the emergence of TL, we performed a perturbative analysis. Motivated by our numerical results, we considered the following ansatzes:

$$x_i(t) = x_0(t - \varepsilon_i \tau) + \varepsilon_i p(t - \varepsilon_i \tau) + O(\varepsilon_i^2), \quad (8a)$$

$$y_i(t) = y_0(t - \varepsilon_i \tau) + \varepsilon_i q(t - \varepsilon_i \tau) + O(\varepsilon_i^2), \quad (8b)$$

$$z_i(t) = z_0(t - \varepsilon_i \tau) + \varepsilon_i r(t - \varepsilon_i \tau) + O(\varepsilon_i^2), \quad (8c)$$

where

$$\varepsilon_i = \frac{\mu_i}{D_y}, \quad (9)$$

denotes nondimensional small parameters; τ is a constant; and $p(t), q(t),$ and $r(t)$ are functions to be determined. We recall that $x_0(t)$ is a periodic function obeying the following relation for the food chain model under consideration:

$$\dot{x}_0 = f_x(x_0, y_0, z_0) = (a - ly_0)x_0 - ax^*. \quad (10)$$

In Eq. (8), waveform proportionality can be said to occur in variable $x_i(t)$ if $p(t) \propto x_0(t)$ holds true in good approximation. As shown below, this is true under some conditions. Substituting Eq. (8) into Eq. (2a) and extracting the $O(\varepsilon_i)$ terms, we obtain:

$$\dot{p} = (a - ly_0 - D_x)p - lqx_0. \quad (11)$$

Notice that Eqs. (10) and (11) are linear in terms of x_0 and p , respectively. Therefore, by assuming that other time-dependent functions are provided, we may solve these equations to obtain the expressions for periodic

$x_0(t)$ and $p(t)$. As shown in Supplemental Material, we obtain:

$$x_0(t) = \left(\kappa_1 - ax^* \int_0^t e^{-\bar{f}t'} g(t') dt' \right) e^{\bar{f}t + \delta F(t)}, \quad (12a)$$

$$p(t) = \left(\kappa_2 - l \int_0^t e^{-(\bar{f} - D_x)t'} h(t') dt' \right) e^{(\bar{f} - D_x)t + \delta F(t)}, \quad (12b)$$

where $\bar{f} = \langle a - ly_0(t) \rangle_t, \delta F(t) = \int_0^t \{f(t') - \bar{f}\} dt', g(t) = e^{-\delta F(t)}$, and $h(t) = q(t)x_0(t)e^{-\delta F(t)}$. κ_1 and κ_2 are arbitrary constants. Note that $\delta F(t)$ is periodic, and thus, $g(t)$ and $h(t)$ are periodic. In the integral provided in Eq. (12a), if the oscillation period of $g(t)$, which is approximately $2\pi/\omega$, is sufficiently smaller than $1/|\bar{f}|$, $e^{-\bar{f}t'}$ is approximately constant during 1 oscillation period, where ω is the oscillation frequency. Then, $g(t)$ can be effectively averaged, and only the average of $g(t)$ is important. By using the Fourier series of $g(t)$, the integral can be directly calculated to obtain:

$$x_0 = \frac{ax^*}{\bar{f}} \left[A + O\left(\frac{\bar{f}}{\omega}\right) \right] e^{\delta F(t)}, \quad (13)$$

where $A = \langle g(t) \rangle_t$. Similarly, we obtain:

$$p = \frac{l}{\bar{f} - D_x} \left[B + O\left(\frac{\bar{f} - D_x}{\omega}\right) \right] e^{\delta F(t)}, \quad (14)$$

where $B = \langle q(t)x_0(t)e^{-\delta F(t)} \rangle_t$. Therefore, $p(t)$ becomes approximately proportional to $x_0(t)$ when the following conditions are satisfied:

$$A \gg O\left(\frac{\bar{f}}{\omega}\right) \text{ and } B \gg O\left(\frac{\bar{f} - D_x}{\omega}\right). \quad (15)$$

Thus, TL with exponent $\beta_{t,s} = 2$ should be observed in good approximation when ε_i is sufficiently small. Furthermore, substituting Eqs. (13) and (14) into Eqs. (4) and (5), and omitting the $O(\cdot)$ terms, we obtain:

$$\alpha_t = \frac{V[e^{\delta F(t)}]_t}{(E[e^{\delta F(t)}]_t)^2}, \quad (16)$$

$$\alpha_s = \left(\frac{\bar{f}}{\bar{f} - D_x} \frac{lB}{ax^*A} \right)^2 V[\varepsilon_i]_i. \quad (17)$$

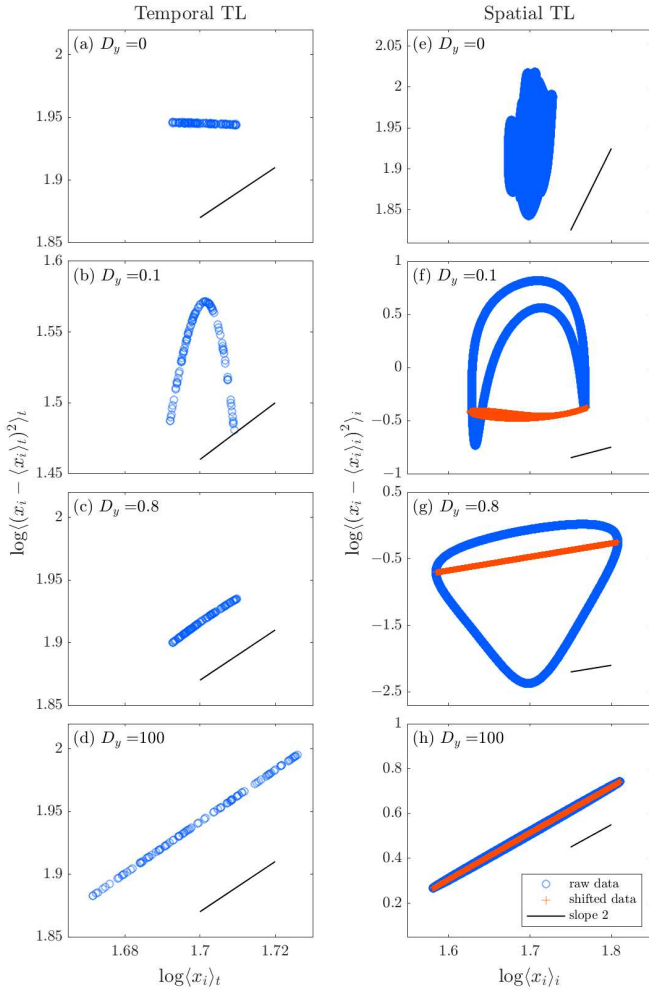


FIG. 2. Examples of TL for each coupling strength. $N = 100$, $D_x = 0$, $D_z = 0$, $a = 1$, $c = 9$, $k = 0.6$, $l = 0.1$, $x^* = 1.6$, $y^* = 0$, and $z^* = 0.01$. b_i was randomly selected from a uniform distribution between 4.9 and 5.1. Temporal and spatial TLs are shown in left and right columns, respectively. Blue plots indicate temporal and spatial TLs for the raw data, red plots indicate spatial TL for the shifted data, and black lines are the reference line with slope 2.

We expect that Eq. (15) can be generally satisfied when \bar{f} and D_x are sufficiently smaller than ω . In the present example, we have $\omega \approx 2.18$, $\bar{f} \approx 0.0327$, and $D_x = 0$, suggesting the validity of our approximation. Indeed, the predicted $\beta_{t,s}$ and $\log \alpha_{t,s}$, shown in black lines in Figs. 3 and S1, are in excellent agreement with the simulation results for large D_y . One might naively expect that waveform proportionality naturally arises for oscillators with strong diffusive coupling because the waveforms become virtually identical in the strong coupling limit. However, note that convergence ($p(t) \rightarrow 0$) does not imply waveform proportionality, and the convergence method is important. An interesting prediction, possibly opposing the naive expectation, is that waveform pro-

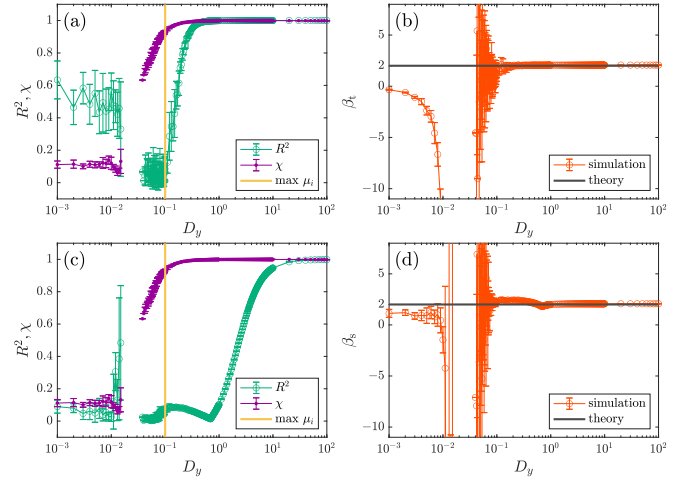


FIG. 3. D_y dependence of TL parameters and synchronization degree of the food chain model. $N = 100$, $D_x = 0$, $D_z = 0$, $a = 1$, $c = 9$, $k = 0.6$, $l = 0.1$, $x^* = 1.6$, $y^* = 0$, and $z^* = 0.01$. b_i was randomly selected from a uniform distribution between 4.9 and 5.1. Simulations were performed up to $t = 3500$, and TL was computed using the time series from $t = 3000$ to $t = 3500$. Error bars represent the standard deviation of 10 calculations with different initial conditions and b_i . In (a) and (c), purple and vertical orange lines represent χ and $\max\{\mu_i\}$, respectively. In (b) and (d), red and black lines represent simulation and theoretical results, respectively. (a) Coefficient of determination of temporal TL (green line). (b) Exponents of temporal TL. (c) Coefficient of determination of spatial TL (green line). (d) Exponents of spatial TL.

portionality is violated when coupling strength D_x in the observed variable is large because this will violate Eq. (15). We numerically demonstrate this prediction in Supplemental Material by considering the $D_x > 0$ cases (Fig. S7). In contrast, there is no condition regarding D_z . Indeed, as demonstrated in Fig. S8, TL is observed for $D_z > 0$.

Next, we generalize our theory considering the following situation. Suppose we have N oscillators, each of which can be described by an M -dimensional dynamical system. Let $x_i(t)$ ($i = 1, \dots, N$) be the observables obeying

$$\dot{x}_i = s_i(t)x_0 + u_i(t), \quad (18)$$

where $s_i(t)$ and $u_i(t)$ are periodic with period $\frac{2\pi}{\omega}$. We assume that $s_i(t) = s(t) + \varepsilon_i \delta s(t)$ and $u_i(t) = u(t) + \varepsilon_i \delta u(t)$ to the lowest order in ε_i , where $s, u, \delta s$, and δu are periodic. Then, the above analysis can similarly be applied to this system. Accordingly, we conclude that waveform proportionality occurs in $x_i(t)$ for small ε_i if Eq. (15), wherein \bar{f} is replaced with $\langle s(t) \rangle_t$, is satisfied. Essentially, the equation should be linear in terms of observables and its intrinsic dynamics should be sufficiently slow. When these assumptions are satisfied, the averaging approximation is effective, resulting in

waveform proportionality. Furthermore, we note that our theory can approximately be extended to a class of chaotic oscillators. Suppose that $s_i(t)$ and $u_i(t)$ in Eq. (18) show chaotic oscillations with characteristic period T . We assume that the time averages of $s_i(t)$ and $u_i(t)$ over 1 period T do not strongly fluctuate from the long-time averages of $s_i(t)$ and $u_i(t)$. Under this assumption, the above arguments hold approximately true. From these observations, we predict that TL can arise in a broad class of systems, including various types of (i) chaotic oscillators, (ii) coupling mechanisms, and (iii) dynamical systems. Concerning (i), as shown in Fig. 4 and Fig. S9, we demonstrate that the same food chain model with another set of parameters that yields chaotic oscillations approximately shows waveform proportionality and TL when the oscillators are synchronized. Concerning (ii), as shown in Fig. S10, we demonstrate that TL is observed in a pacemaker-driven system, where $Y = y_0$ in Eq. (2). Concerning (iii), as an example, we consider the following Rössler system [39–44]: $f_x = -(\omega_0 + \mu_i)y_i - z_i$, $f_y = (\omega_0 + \mu_i)x_i + ay_i$, and $f_z = b + z_i(x_i - c)$ in Eq. (2), where we employ the standard parameter values as $a = 0.1$, $b = 0.1$, and $c = 0.7$, and introduce μ_i as a heterogeneity parameter. Following previous works [39–44], we consider $D_x = D_y = D > 0$ and $D_z = 0$. The simulation results of the Rössler system are shown in Fig. S11. Note that the actual frequency, ω , is approximately ω_0 in this system. In this system, TL is expected to be observed in variable z because Eq. (15), wherein D_x and \bar{f} are replaced with 0 and $\langle x_i(t) - c \rangle_t$, respectively, may be satisfied for any value of D . Furthermore, we investigate ω_0 dependency in addition to D dependency because the validity of Eq. (15) can conveniently be controlled through ω_0 . We investigate ω_0 dependency for fixed $D = 100$. As expected, exponent $\beta_{t,s}$ approaches 2 with large coefficients of determination (R^2) as ω_0 increases (Fig. S12).

Discussion. In this study, we showed that temporal and spatial TLs are induced by synchronization in a broad class of periodic and chaotic oscillators. Specifically, we demonstrated that as the degree of synchronization increases, the correlation between $\log(\text{mean})$ and $\log(\text{variance})$ becomes stronger. Moreover, we showed that in regions of strong synchronization, waveform proportionality emerges, resulting in the derivation of temporal and spatial TLs with exponent 2. In these synchronization-induced TLs, temporal and spatial TLs arise in the same mechanism, i.e., waveform proportionality. In contrast, owing to phase lag, which is expressed by the $\varepsilon_i\tau$ terms in Eq. (8), spatial TL requires stronger coupling than temporal TL. While several studies explored the relationship between TL and synchronization [7, 18, 22–24, 28, 30, 31, 36, 45], the details of the relationship are not fully understood yet. Many of these studies investigated the correlation between the

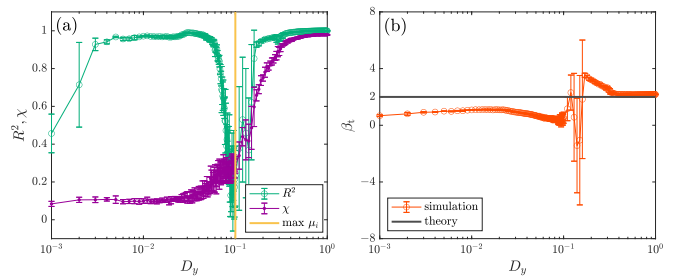


FIG. 4. D_y dependence of TL parameters and synchronization degree of the food chain model in chaotic region. $N = 100$, $a = 1$, $c = 10$, $k = 0.6$, $l = 0.1$, $x^* = 1.5$, $y^* = 0$, and $z^* = 0.01$. b_i was randomly selected from a uniform distribution between 0.9 and 1.1. Simulations were performed up to $t = 3500$, and TL was computed using the time series from $t = 3000$ to $t = 3500$. Error bars represent the standard deviation of 10 calculations with different initial conditions and b_i . In (a), purple and vertical orange lines represent χ and $\max\{\mu_i\}$, respectively. In (b), red and black lines represent simulation and theoretical results, respectively. (a) Coefficient of determination of temporal TL (green line). (b) Exponents of temporal TL.

exponents of TL and degree of synchronization through numerical simulations [22, 24, 28, 30, 31, 36]. In refs. [7, 22, 23], the authors argued that temporal TL with exponent 2 is observed when the time series are perfectly correlated. Reuman et al. derived the analytical relationship between spatial TL and synchronization [18]. In this study, we analytically derived both temporal and spatial TLs with exponent 2 from the synchronization state in a broad class of periodic and chaotic oscillators. Although other mechanisms are known to exist for TL with exponent 2 [3, 19, 21, 25, 27, 29, 32–34], and the synchronization considered in this study is slightly unusual owing to its intensity and special correlation (waveform proportionality), we believe that our findings provide valuable insights into the understanding of TL from the perspective of synchronization as another universal phenomenon in ecosystems [46]. Our study can help in inferring the existence of synchronization solely from the relationship between the mean and variance [47].

Similar phenomena as waveform proportionality have been proposed previously, including the projective synchronization [48] and a type of generalized synchronization [49]. These previously reported phenomena are observed in a limited class of coupled oscillators. We showed that waveform proportionality arises in a broad class of coupled periodic or chaotic oscillators when the oscillators are strongly synchronized.

This study was supported by JSPS KAKENHI Grant Number JP23KJ0830 and WINGS CFS program of The Univ. of Tokyo to Y.M., and JSPS KAKENHI Grant Number JP21K12056 to H.K.

-
- * mitsui@g.ecc.u-tokyo.ac.jp
† kori@k.u-tokyo.ac.jp
- [1] C. I. Bliss, *J. Econ. Entomol.* **34**, 221 (1941).
[2] L. R. Taylor, *Nature* **189**, 732 (1961).
[3] A. S. Sassi, M. Garcia-Alcala, M. Aldana, and Y. Tu, *Phys. Rev. X* **12**, 011051 (2022).
[4] M. A. de Menezes and A. L. Barabási, *Phys. Rev. Lett.* **92**, 028701 (2004).
[5] M. A. D. Menezes and A. L. Barabási, *Phys. Rev. Lett.* **93**, 068701 (2004).
[6] J. Duch and A. Arenas, *Phys. Rev. Lett.* **96**, 218702 (2006).
[7] Z. Eisler, I. Bartos, and J. Kertész, *Adv. Phys.* **57**, 89 (2008).
[8] R. A. J. Taylor, *Taylor's Power Law: Order and Pattern in Nature*, 1st ed. (Academic Press, 2019).
[9] V. Narayan, S. Ramaswamy, and N. Menon, *Science* **317**, 105 (2007).
[10] D. Das, D. Das, and A. Prasad, *J. Theor. Biol.* **308**, 96 (2012).
[11] B. Houchmandzadeh, *Phys. Rev. E* **98**, 042118 (2018).
[12] B. Mahault, F. Ginelli, and H. Chaté, *Phys. Rev. Lett.* **123**, 218001 (2019).
[13] J. Toner and Y. Tu, *Phys. Rev. Lett.* **75**, 4326 (1995).
[14] F. Ginelli, *Eur. Phys. J. Special Topics* **225**, 2099 (2016).
[15] H. Chaté, *Annu. Rev. Condens. Matter Phys.* **11**, 189 (2020).
[16] D. Nishiguchi, *J. Phys. Soc. Jpn.* **92**, 121007 (2023).
[17] J. N. Perry, *Proc. Royal Soc. B* **257**, 221 (1994).
[18] D. C. Reuman, L. Zhao, L. W. Sheppard, P. C. Reid, and J. E. Cohen, *Proc. Natl. Acad. Sci. U.S.A.* **114**, 6788 (2017).
[19] A. Giometto, M. Formentin, A. Rinaldo, J. E. Cohen, and A. Maritan, *Proc. Natl. Acad. Sci. U.S.A.* **112**, 7755 (2015).
[20] J. E. Cohen and M. Xu, *Proc. Natl. Acad. Sci. U.S.A.* **112**, 7749 (2015).
[21] F. Ballantyne IV, *Evol. Ecol. Res.* **7**, 1213 (2005).
[22] F. Ballantyne IV and A. J. Kerkhoff, *J. Theor. Biol.* **235**, 373 (2005).
[23] F. Ballantyne IV and A. J. Kerkhoff, *Oikos* **116**, 174 (2007).
[24] A. J. Kerkhoff and F. Ballantyne IV, *Ecol. Lett.* **6**, 850 (2003).
[25] J. E. Cohen, *Theor. Ecol.* **7**, 77 (2014).
[26] J. E. Cohen, *Theor. Popul. Biol.* **93**, 30 (2014).
[27] J. E. Cohen, M. Xu, and W. S. Schuster, *Proc. Royal Soc. B* **280** (2013).
[28] L. Zhao, L. W. Sheppard, P. C. Reid, J. A. Walter, and D. C. Reuman, *J. Anim. Ecol.* **88**, 484 (2019).
[29] J. E. Cohen, *Theor. Popul. Biol.* **88**, 94 (2013).
[30] J. E. Cohen and T. Saitoh, *Ecology* **97**, 3402 (2016).
[31] T. Saitoh, *Popul. Ecol.* **62**, 300 (2020).
[32] R. M. Anderson, D. M. Gordon, M. J. Crawley, and M. P. Hassel, *Nature* **296**, 245 (1982).
[33] A. M. Kilpatrick and A. R. Ives, *Nature* **422**, 65 (2003).
[34] S. Carpenter, S. Callens, C. Brown, J. E. Cohen, and B. Z. Webb, *Theor. Popul. Biol.* **154**, 118 (2023).
[35] L. R. Taylor and I. P. Woiwod, *J. Anim. Ecol.* **51**, 879 (1982).
[36] I. Hanski, *Oikos* **50**, 148 (1987).
[37] B. Blasius, A. Huppert, and L. Stone, *Nature* **399**, 354 (1999).
[38] B. Blasius and L. Stone, *Int. J. Bifurcat. Chaos* **10** (2000).
[39] E. Montbrió and B. Blasius, *Chaos* **13**, 291 (2003).
[40] M. G. Rosenblum, A. S. Pikovsky, and J. Kurths, *Phys. Rev. Lett.* **76**, 1804 (1996).
[41] M. G. Rosenblum, A. S. Pikovsky, and J. Kurths, *Phys. Rev. Lett.* **78**, 4193 (1997).
[42] H. Sakaguchi, *Phys. Rev. E* **61**, 7212 (2000).
[43] A. S. Pikovsky, M. G. Rosenblum, and J. Kurths, *Europhys. Lett.* **34**, 165 (1996).
[44] G. V. Osipov, A. S. Pikovsky, M. G. Rosenblum, and J. R. Kurths, *Phase synchronization effects in a lattice of nonidentical rössler oscillators* (1997).
[45] I. Hanski and I. P. Woiwod, *J. Anim. Ecol.* **62**, 656 (1993).
[46] A. Liebhold, W. D. Koenig, and O. N. Bjørnstad, *Annu. Rev. Ecol. Evol. Sys* **35**, 467 (2004).
[47] G. Petri, P. Expert, H. J. Jensen, and J. W. Polak, *Sci. Rep.* **3** (2013).
[48] R. Mainieri and J. Rehacek, *Phys. Rev. Lett.* **82**, 3042 (1999).
[49] T. Kano and K. Umeno, *Chaos* **32**, 113137 (2022).

Supplemental Material: Waveform Proportionality and Taylor's Law Induced by Synchronization of Periodic and Chaotic Oscillators

Yuzuru Mitsui* and Hiroshi Kori†
 Graduate School of Frontier Sciences, The University of Tokyo
 (Dated: November 27, 2023)

FIGURES

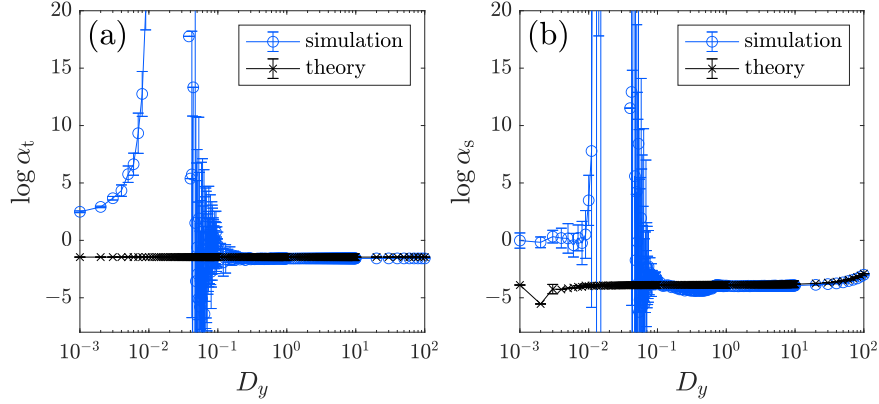


Fig. S1. D_y dependence of $\log \alpha_{t,s}$ of the food chain model. $N = 100, D_x = 0, D_z = 0, a = 1, c = 9, k = 0.6, l = 0.1, x^* = 1.6, y^* = 0,$ and $z^* = 0.01$. b_i was randomly selected from a uniform distribution between 4.9 and 5.1. Simulations were performed up to $t = 3500$, and TL was computed using the time series from $t = 3000$ to $t = 3500$. Error bars represent the standard deviation of 10 calculations with different initial conditions and b_i . In (a) and (b), blue and black lines represent simulation and theoretical results, respectively. (a) Intercepts of temporal TL. (b) Intercepts of spatial TL.

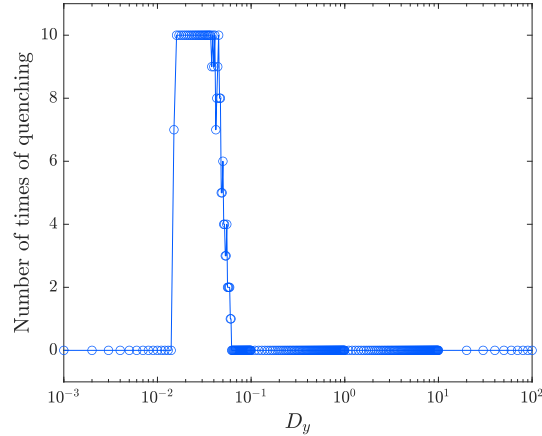


Fig. S2. The number of times we judged that quenching occurred for each coupling strength D_y for the food chain model. $N = 100, D_x = 0, D_z = 0, a = 1, c = 9, k = 0.6, l = 0.1, x^* = 1.6, y^* = 0,$ and $z^* = 0.01$. b_i was randomly selected from a uniform distribution between 4.9 and 5.1. We judged quenching occurred when $1/N \sum_{i=1}^N \langle (x_i(t) - \langle x_i(t) \rangle_t)^2 \rangle_t < 0.001$. Simulations were performed up to $t = 3500$, and the time series from $t = 3000$ to $t = 3500$ were used for the calculations.

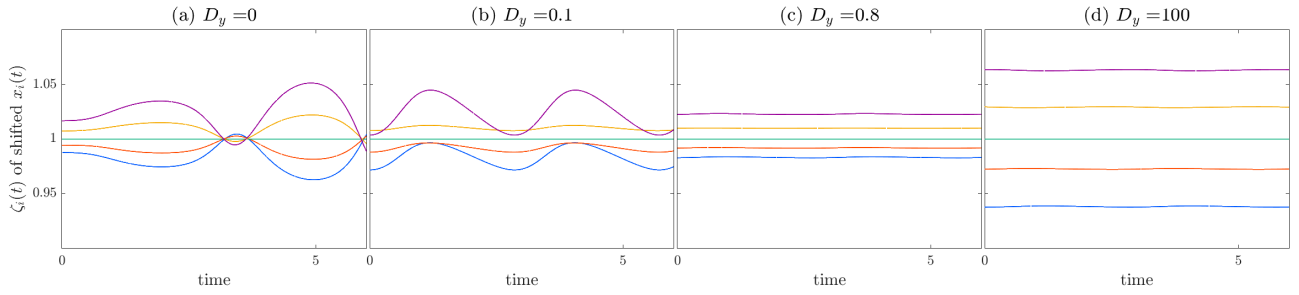


Fig. S3. Examples of $\zeta_i(t)$ of shifted $x_i(t)$ for each coupling strength. $N = 100$, $D_x = 0$, $D_z = 0$, $a = 1$, $c = 9$, $k = 0.6$, $l = 0.1$, $x^* = 1.6$, $y^* = 0$, and $z^* = 0.01$. b_i was randomly selected from a uniform distribution between 4.9 and 5.1. Data for $i = 1, 25, 50, 75$, and 100 are shown.

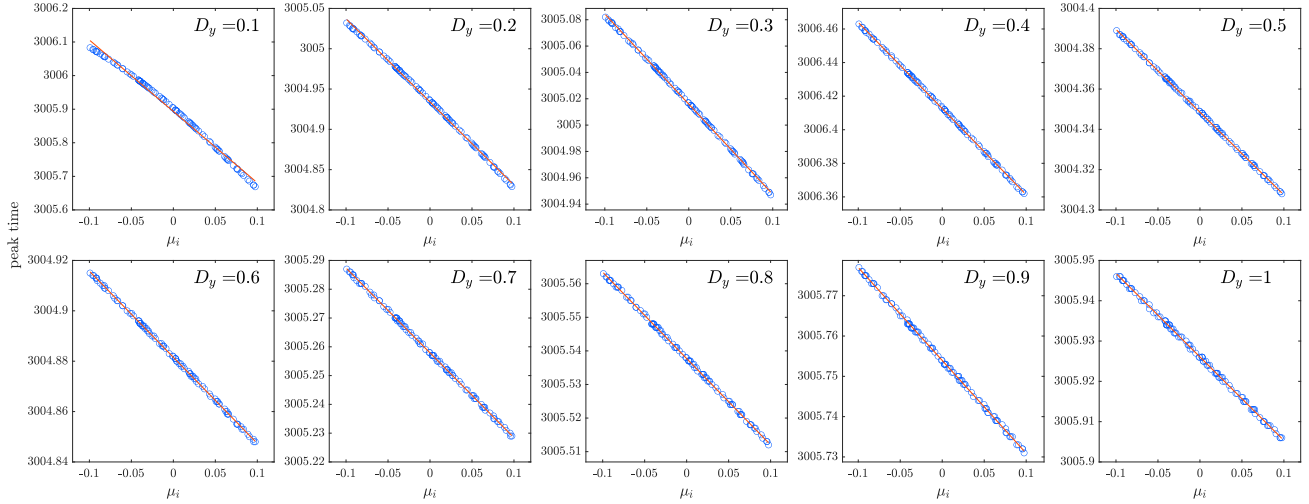


Fig. S4. Phase lag analysis for μ_i . $N = 100$, $D_x = 0$, $D_z = 0$, $a = 1$, $c = 9$, $k = 0.6$, $l = 0.1$, $x^* = 1.6$, $y^* = 0$, and $z^* = 0.01$. b_i was randomly selected from a uniform distribution between 4.9 and 5.1. The vertical axis means the times when each $x_i(t)$ reaches its local maximum value.

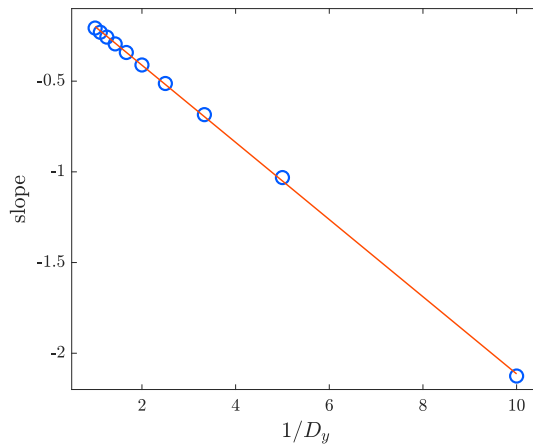


Fig. S5. Phase lag analysis for $1/D_y$. $N = 100$, $D_x = 0$, $D_z = 0$, $a = 1$, $c = 9$, $k = 0.6$, $l = 0.1$, $x^* = 1.6$, $y^* = 0$, and $z^* = 0.01$. b_i was randomly selected from a uniform distribution between 4.9 and 5.1. The vertical axis represents the slope of the approximate straight lines of the 10 graphs shown in Fig. S4.

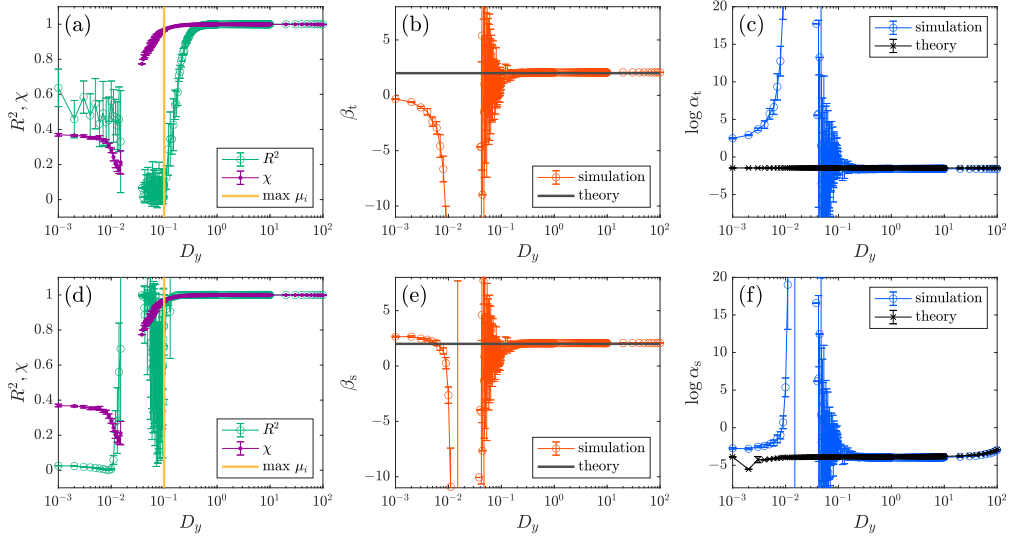


Fig. S6. When TL is computed after applying phase shifts to the time series so that the peaks coincide, the onsets of temporal and spatial TLs almost overlap. $N = 100$, $D_x = 0$, $D_z = 0$, $a = 1$, $c = 9$, $k = 0.6$, $l = 0.1$, $x^* = 1.6$, $y^* = 0$, and $z^* = 0.01$. b_i was randomly selected from a uniform distribution between 4.9 and 5.1. Simulations were performed up to $t = 3500$, and TL was computed using the time series from $t = 3000$ to $t = 3500$. Error bars represent the standard deviation of 10 calculations with different initial conditions and b_i . In (a) and (d), purple and vertical orange lines represent χ and $\max\{\mu_i\}$, respectively. In (b) and (e), red and black lines represent simulation and theoretical results, respectively. In (c) and (f), blue and black lines represent simulation and theoretical results, respectively. (a) Coefficient of determination of temporal TL (green line). (b) Exponents of temporal TL. (c) Intercepts of temporal TL. (d) Coefficient of determination of spatial TL (green line). (e) Exponents of spatial TL. (f) Intercepts of spatial TL.

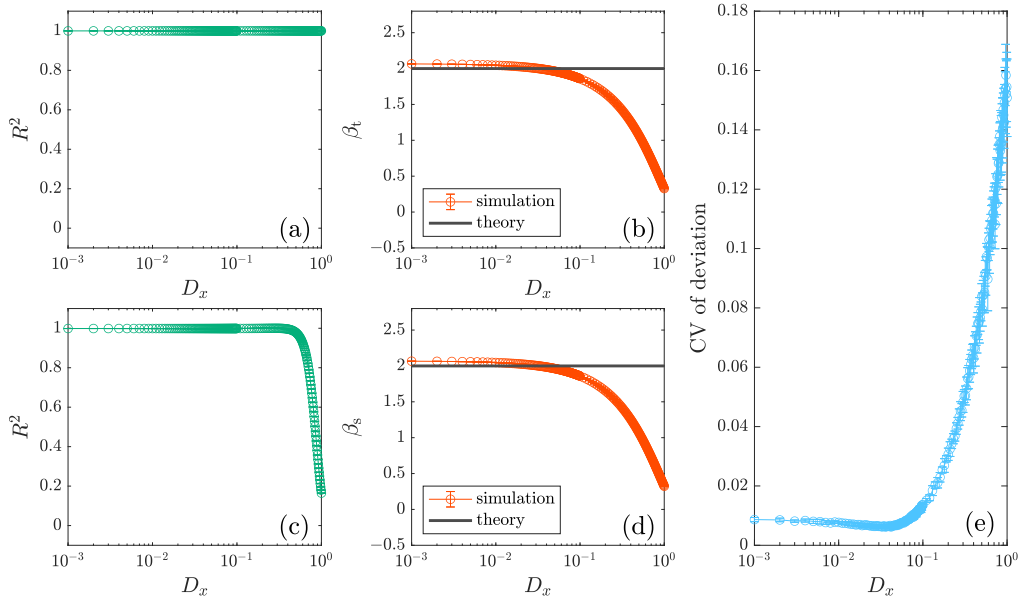


Fig. S7. Simulation results with fixed $D_y (= 100)$ value and varying D_x . To evaluate waveform proportionality, set $x_i = x_0 + \varepsilon_i(p + w)$. If waveform proportionality appears, then $p + w$ should be proportional to x_0 . Thus we calculated the coefficient of variation of $(p + w)/x_0 = D_y/\mu_i(x_i/x_0 - 1)$. Note that x_{50} was used instead of x_0 in the actual calculation. $N = 100$, $D_z = 0$, $a = 1$, $c = 9$, $k = 0.6$, $l = 0.1$, $x^* = 1.6$, $y^* = 0$, and $z^* = 0.01$. b_i was randomly selected from a uniform distribution between 4.9 and 5.1. Error bars represent the standard deviation of 10 calculations with different initial conditions and b_i . (a) Coefficient of determination of temporal TL. (b) Exponents of temporal TL. (c) Coefficient of determination of spatial TL. (d) Exponents of spatial TL. (e) Coefficient of variation of the deviation. $\frac{1}{N-1} \sum_{i \neq 50} \text{CV}[D_y/\mu_i(x_i/x_{50} - 1)]$ is plotted.

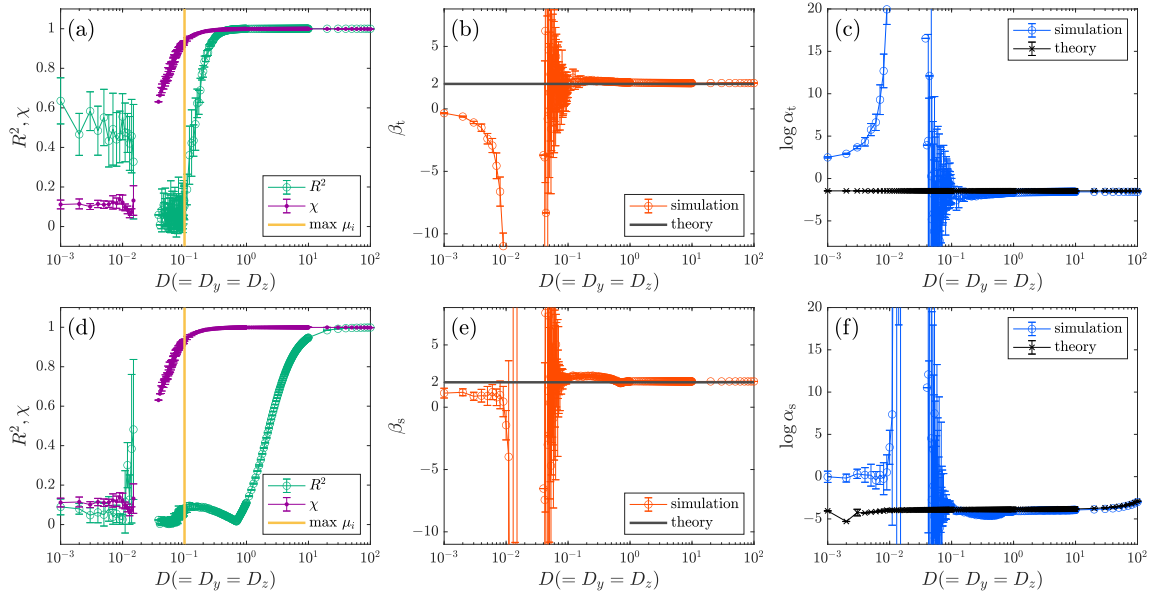


Fig. S8. $D(= D_y = D_z)$ dependence of TL parameters and synchronization degree of the food chain model with coupling at y_i and z_i . $N = 100, D_x = 0, a = 1, c = 9, k = 0.6, l = 0.1, x^* = 1.6, y^* = 0$, and $z^* = 0.01$. b_i was randomly selected from a uniform distribution between 4.9 and 5.1. Simulations were performed up to $t = 3500$, and TL was computed using the time series from $t = 3000$ to $t = 3500$. Error bars represent the standard deviation of 10 calculations with different initial conditions and b_i . In (a) and (d), purple and vertical orange lines represent χ and $\max\{\mu_i\}$, respectively. In (b) and (e), red and black lines represent simulation and theoretical results, respectively. In (c) and (f), blue and black lines represent simulation and theoretical results, respectively. (a) Coefficient of determination of temporal TL (green line). (b) Exponents of temporal TL. (c) Intercepts of temporal TL. (d) Coefficient of determination of spatial TL (green line). (e) Exponents of spatial TL. (f) Intercepts of spatial TL.

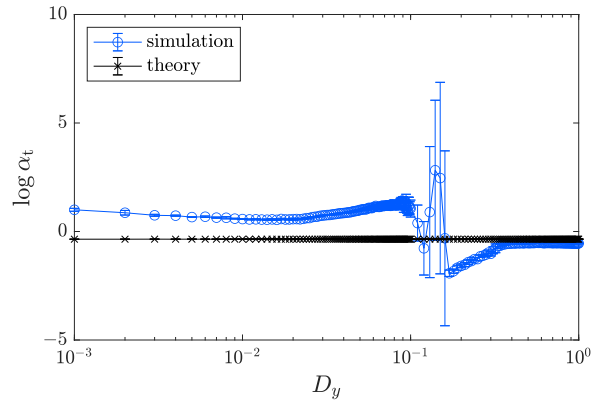


Fig. S9. D_y dependence of $\log \alpha_t$ of the food chain model in chaotic region. $N = 100, D_x = 0, D_z = 0, a = 1, c = 10, k = 0.6, l = 0.1, x^* = 1.5, y^* = 0$, and $z^* = 0.01$. b_i was randomly selected from a uniform distribution between 0.9 and 1.1. Simulations were performed up to $t = 3500$, and TL was computed using the time series from $t = 3000$ to $t = 3500$. Error bars represent the standard deviation for 10 calculations with different initial conditions and b_i . Blue and black lines represent simulation and theoretical results, respectively.

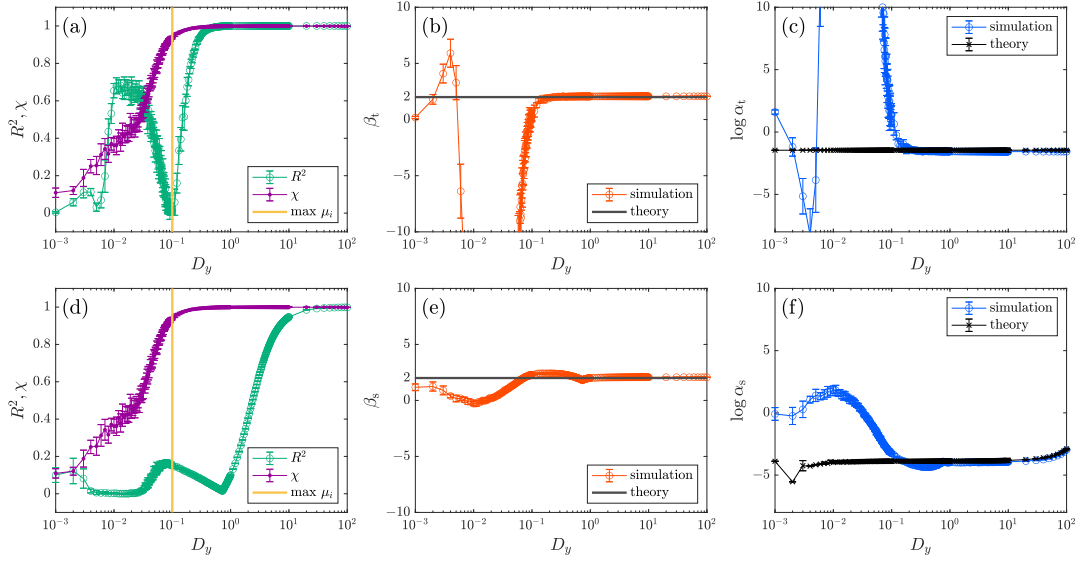


Fig. S10. D_y dependence of TL parameters and synchronization degree of the pacemaker-driven food chain model. $N = 100$, $D_x = 0$, $D_z = 0$, $a = 1$, $c = 9$, $k = 0.6$, $l = 0.1$, $x^* = 1.6$, $y^* = 0$, and $z^* = 0.01$. b_i was randomly selected from a uniform distribution between 4.9 and 5.1. Simulations were performed up to $t = 3500$, and TL was computed using the time series from $t = 3000$ to $t = 3500$. Error bars represent the standard deviation of 10 calculations with different initial conditions and b_i . In (a) and (d), purple and vertical orange lines represent χ and $\max\{\mu_i\}$, respectively. In (b) and (e), red and black lines represent simulation and theoretical results, respectively. In (c) and (f), blue and black lines represent simulation and theoretical results, respectively. (a) Coefficient of determination of temporal TL (green line). (b) Exponents of temporal TL. (c) Intercepts of temporal TL. (d) Coefficient of determination of spatial TL (green line). (e) Exponents of spatial TL. (f) Intercepts of spatial TL.

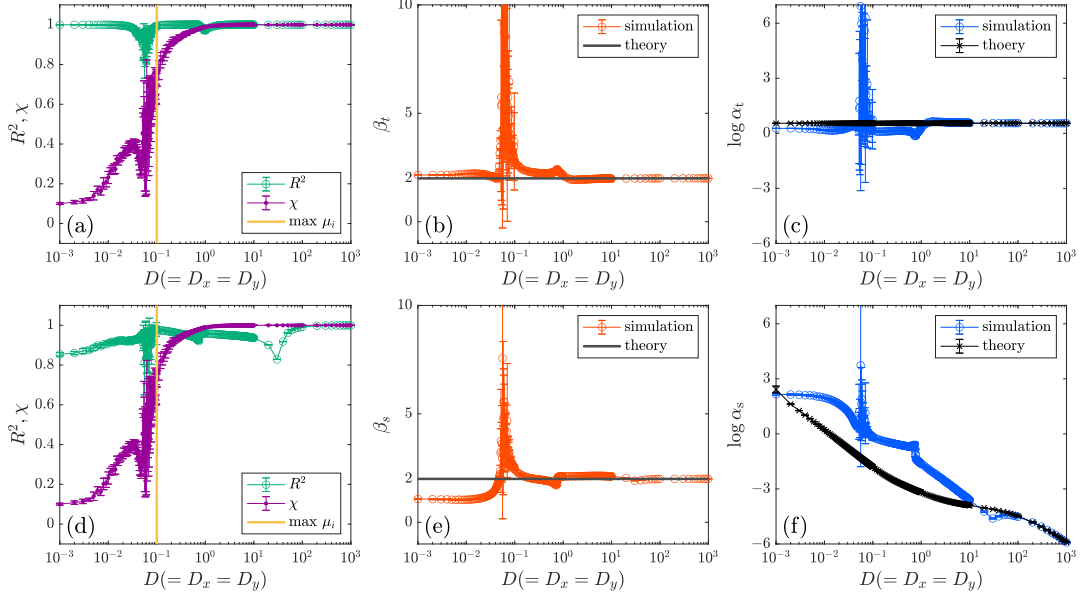


Fig. S11. $D(= D_x = D_y)$ dependence of TL parameters and synchronization degree of the Rössler system. $N = 100$, $D_z = 0$, $a = 0.1$, $b = 0.1$ and $c = 0.7$. ω_i was randomly selected from a uniform distribution between 5.4 and 5.6. Simulations were performed up to $t = 3500$, and TL was computed using the time series from $t = 3000$ to $t = 3500$. Error bars represent the standard deviation of 10 calculations with different initial conditions and ω_i . In (a) and (d), purple and vertical orange lines represent χ and $\max\{\mu_i\}$, respectively. In (b) and (e), red and black lines represent simulation and theoretical results, respectively. In (c) and (f), blue and black lines represent simulation and theoretical results, respectively. (a) Coefficient of determination of temporal TL (green line). (b) Exponents of temporal TL. (c) Intercepts of temporal TL. (d) Coefficient of determination of spatial TL (green line). (e) Exponents of spatial TL. (f) Intercepts of spatial TL.

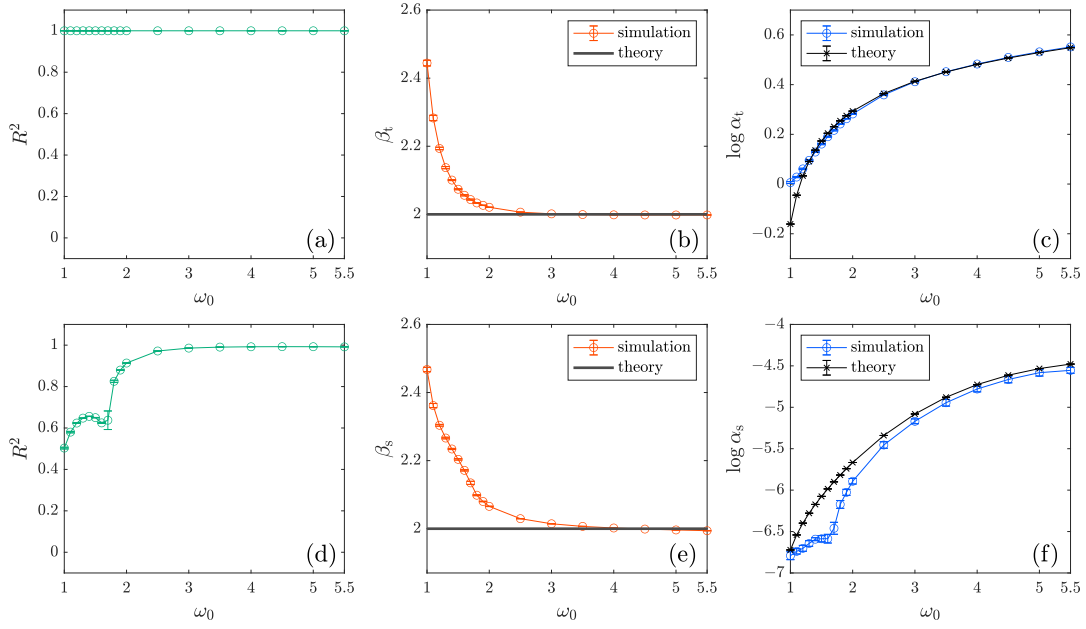


Fig. S12. ω_0 dependence of TL parameters of the Rössler system. $N = 100, D_x = D_y = 100, D_z = 0, a = 0.1, b = 0.1$ and $c = 0.7$. ω_i was randomly selected from a uniform distribution between $(\omega_0 - 0.1)$ and $(\omega_0 + 0.1)$. Simulations were performed up to $t = 3500$, and TL was computed using the time series from $t = 3000$ to $t = 3500$. Error bars represent the standard deviation of 10 calculations with different initial conditions and ω_i . In (b) and (e), red and black lines represent simulation and theoretical results, respectively. In (c) and (f), blue and black lines represent simulation and theoretical results, respectively. (a) Coefficient of determination of temporal TL. (b) Exponents of temporal TL. (c) Intercepts of temporal TL. (d) Coefficient of determination of spatial TL. (e) Exponents of spatial TL. (f) Intercepts of spatial TL.

CALCULATION DETAILS

$$\dot{x}_i = a(x_i - x^*) - lx_i y_i + \frac{D_x}{N} \sum_{j=1}^N (x_j - x_i), \quad (1)$$

$$\dot{y}_i = -b_i(y_i - y^*) + lx_i y_i - ky_i z_i + \frac{D_y}{N} \sum_{j=1}^N (y_j - y_i), \quad (2)$$

$$\dot{z}_i = -c(z_i - z^*) + ky_i z_i + \frac{D_z}{N} \sum_{j=1}^N (z_j - z_i), \quad (3)$$

where,

$$b_i = b_0 + \mu_i, \quad (4)$$

$$\langle \mu_i \rangle_i = 0. \quad (5)$$

Assume that the solutions are as follows:

$$x_i(t) = x_0(t) + \frac{\mu_i}{D_y} p(t), \quad (6)$$

$$y_i(t) = y_0(t) + \frac{\mu_i}{D_y} q(t), \quad (7)$$

$$z_i(t) = z_0(t) + \frac{\mu_i}{D_y} r(t), \quad (8)$$

where, $x_0, y_0,$ and z_0 satisfy the following:

$$\dot{x}_0 = a(x_0 - x^*) - lx_0 y_0, \quad (9)$$

$$\dot{y}_0 = -b_0(y_0 - y^*) + lx_0 y_0 - ky_0 z_0, \quad (10)$$

$$\dot{z}_0 = -c(z_0 - z^*) + ky_0 z_0. \quad (11)$$

Substituting Eqs. (6) and (7) into Eq. (1), we obtain,

$$\dot{x}_0 + \varepsilon_i \dot{p} = ax_0 + \varepsilon_i ap - ax^* - lx_0 y_0 - \varepsilon_i l q x_0 - \varepsilon_i l p y_0 - \varepsilon_i^2 l p q + D_x x_0 - D_x x_0 - D_x \varepsilon_i p, \quad (12)$$

$$\therefore \varepsilon_i \dot{p} = \varepsilon_i ap - \varepsilon_i l q x_0 - \varepsilon_i l p y_0 - \varepsilon_i^2 l p q - \varepsilon_i D_x p, \quad (13)$$

where $\varepsilon_i = \mu_i/D_y$. Comparing both sides for ε_i , we obtain,

$$\dot{p} = (a - ly_0 - D_x)p - lq x_0. \quad (14)$$

Substituting Eqs. (6), (7), and (8) into Eq. (2), we obtain,

$$\dot{y}_0 + \varepsilon_i \dot{q} = -b_0 y_0 - \varepsilon_i b_0 q + b_0 y^* - \mu_i y_0 - \mu_i \varepsilon_i q + \mu_i y^* \quad (15)$$

$$+ lx_0 y_0 + \varepsilon_i l q x_0 + \varepsilon_i l p y_0 + \varepsilon_i^2 l p q - ky_0 z_0 - \varepsilon_i k r y_0 - \varepsilon_i k q z_0 - \varepsilon_i^2 k q r + D_y y_0 - D_y y_0 - \varepsilon_i D_y q, \quad (16)$$

$$\therefore \varepsilon_i \dot{q} = -\varepsilon_i b_0 q - \varepsilon_i D_y y_0 - \varepsilon_i^2 D_y q + \mu_i y^* + \varepsilon_i l q x_0 + \varepsilon_i l p y_0 + \varepsilon_i^2 l p q - \varepsilon_i k r y_0 - \varepsilon_i k q z_0 - \varepsilon_i^2 k q r - \varepsilon_i D_y q. \quad (17)$$

Comparing both sides for ε_i , we obtain,

$$\dot{q} = (-b_0 + lx_0 - kz_0 - D_y)q + (-D_y + lp - kr)y_0 + D_y y^*. \quad (18)$$

Substituting Eqs. (7) and (8) into Eq. (3), we obtain,

$$\dot{z}_0 + \varepsilon_i \dot{r} = -cz_0 - \varepsilon_i cr + cz^* + ky_0 z_0 + \varepsilon_i k r y_0 + \varepsilon_i k q z_0 + \varepsilon_i^2 k q r + D_z z_0 - D_z z_0 - \varepsilon_i D_z r, \quad (19)$$

$$\therefore \varepsilon_i \dot{r} = -\varepsilon_i cr + \varepsilon_i k r y_0 + \varepsilon_i k q z_0 + \varepsilon_i^2 k q r - \varepsilon_i D_z r. \quad (20)$$

Comparing both sides for ε_i , we obtain,

$$\dot{r} = (-c + ky_0 - D_z)r + kqz_0. \quad (21)$$

Thus, the dynamics of p, q , and r are as follows:

$$\dot{p} = (a - ly_0 - D_x)p - lqx_0, \quad (22)$$

$$\dot{q} = (-b_0 + lx_0 - kz_0 - D_y)q + (-D_y + lp - kr)y_0 + D_y y^*, \quad (23)$$

$$\dot{r} = (-c + ky_0 - D_z)r + kqz_0. \quad (24)$$

By assuming that $y_0(t)$ is a given periodic function with period T and solving Eqs. (9) and (22), we are going to show that $x_0(t)$ and $p(t)$ are approximately proportional under a certain condition to be determined. We introduce

$$f(t) = a - ly_0, \quad (25)$$

$$\bar{f} = \langle f(t) \rangle_t, \quad (26)$$

$$\delta f(t) = f(t) - \bar{f}, \quad (27)$$

$$\delta F(t) = \int_0^t \delta f(t') dt'. \quad (28)$$

Note that $\delta F(t)$ is a periodic function with period T . The general solution $x_0(t)$ to Eq. (9) for given $y_0(t)$ is given as

$$x_0(t) = \left(\kappa_1 - ax^* \int_0^t e^{-\bar{f}t' - \delta F(t')} dt' \right) e^{\bar{f}t + \delta F(t)}, \quad (29)$$

where κ_1 is an arbitrary constant. We expand $e^{-\delta F(t)}$ in the Fourier series:

$$e^{-\delta F(t)} = A + \sum_{n=1}^{\infty} \{a_n \cos(\omega n t) + b_n \sin(\omega n t)\}, \quad (30)$$

where $\omega = \frac{2\pi}{T}$; and A, a_n , and b_n are Fourier coefficients. In particular, note that

$$A = \langle e^{-\delta F(t)} \rangle_t. \quad (31)$$

Using Eq. (30), we obtain

$$\int_0^t e^{-\bar{f}t' - \delta F(t')} dt' = e^{-\bar{f}t} \left[-\frac{A}{\bar{f}} + \sum_{n=1}^{\infty} \frac{(a_n \omega n - b_n \bar{f}) \sin(\omega n t) - (a_n \bar{f} + b_n \omega n) \cos(\omega n t)}{\bar{f}^2 + (\omega n)^2} \right] \quad (32)$$

$$+ \sum_{n=1}^{\infty} \frac{a_n \bar{f} + b_n \omega n}{\bar{f}^2 + (\omega n)^2} + \frac{A}{\bar{f}}. \quad (33)$$

By setting

$$\tilde{\kappa}_1 = \kappa_1 - ax^* \sum_{n=1}^{\infty} \frac{a_n \bar{f} + b_n \omega n}{\bar{f}^2 + (\omega n)^2} - ax^* \frac{A}{\bar{f}}, \quad (34)$$

we obtain

$$x_0(t) = \left[\tilde{\kappa}_1 - ax^* e^{-\bar{f}t} \left\{ -\frac{A}{\bar{f}} + \sum_{n=1}^{\infty} \frac{(a_n \omega n - b_n \bar{f}) \sin(\omega n t) - (a_n \bar{f} + b_n \omega n) \cos(\omega n t)}{\bar{f}^2 + (\omega n)^2} \right\} \right] e^{\bar{f}t + \delta F(t)}. \quad (35)$$

Since we are concerned with periodic $x_0(t)$, we set $\tilde{\kappa}_1 = 0$. We assume that $\bar{f} \ll \omega$. Then, we can estimate

$$x_0 = \frac{ax^*}{\bar{f}} \left[A + O\left(\frac{\bar{f}}{\omega}\right) \right] e^{\delta F(t)}. \quad (36)$$

Therefore, when

$$A \gg \left| \frac{\bar{f}}{\omega} \right|, \quad (37)$$

$x_0(t)$ is well approximated to

$$x_0(t) \approx \frac{ax^*A}{f} e^{\delta F(t)}. \quad (38)$$

Next, by solving Eq. (22) for given periodic $x_0(t), y_0(t)$ and $q(t)$, we obtain an expression for $p(t)$. The general solution is given as

$$p(t) = \left(\kappa_2 - l \int_0^t q(t') x_0(t') e^{-(\bar{f}-D_x)t' - \delta F(t')} dt' \right) e^{(\bar{f}-D_x)t + \delta F(t)}. \quad (39)$$

We expand

$$q(t)x_0(t)e^{-\delta F(t)} = B + \sum_{n=1}^{\infty} \{c_n \cos(\omega n t) + d_n \sin(\omega n t)\}, \quad (40)$$

where B, c_n , and d_n are Fourier coefficients. In particular, note that

$$B = \langle q(t)x_0(t)e^{-\delta F(t)} \rangle_t. \quad (41)$$

Using Eq. (40), we obtain

$$\int_0^t q(t') x_0(t') e^{-\bar{f}t' + D_x t' - \delta F(t')} dt' \quad (42)$$

$$= e^{(D_x - \bar{f})t} \left[\frac{B}{D_x - \bar{f}} + \sum_{n=1}^{\infty} \frac{\{c_n(D_x - \bar{f}) - d_n \omega n\} \cos(\omega n t) + \{c_n \omega n + d_n(D_x - \bar{f})\} \sin(\omega n t)}{(D_x - \bar{f})^2 + (\omega n)^2} \right] \quad (43)$$

$$+ \sum_{n=1}^{\infty} \frac{d_n \omega n - c_n(D_x - \bar{f})}{(D_x - \bar{f})^2 + (\omega n)^2} - \frac{B}{D_x - \bar{f}}. \quad (44)$$

By setting

$$\tilde{\kappa}_2 = \kappa_2 - l \sum_{n=1}^{\infty} \frac{d_n \omega n - c_n(D_x - \bar{f})}{(D_x - \bar{f})^2 + (\omega n)^2} + \frac{lB}{D_x - \bar{f}}, \quad (45)$$

we obtain

$$p(t) = \left[\tilde{\kappa}_2 - l e^{(D_x - \bar{f})t} \left\{ \frac{B}{D_x - \bar{f}} + \sum_{n=1}^{\infty} \frac{\{c_n(D_x - \bar{f}) - d_n \omega n\} \cos(\omega n t) + \{c_n \omega n + d_n(D_x - \bar{f})\} \sin(\omega n t)}{(D_x - \bar{f})^2 + (\omega n)^2} \right\} \right] e^{(\bar{f}-D_x)t + \delta F(t)}. \quad (46)$$

Since we are concerned with periodic $p(t)$, we set $\tilde{\kappa}_2 = 0$. Similarly to $x_0(t)$, we obtain

$$p = \frac{l}{\bar{f} - D_x} \left[B + O\left(\frac{\bar{f} - D_x}{\omega}\right) \right] e^{\delta F(t)}. \quad (47)$$

We thus find that when

$$B \gg \left| \frac{\bar{f} - D_x}{\omega} \right|, \quad (48)$$

$p(t)$ is well approximated to

$$p(t) \approx \frac{lB}{\bar{f} - D_x} e^{\delta F(t)}, \quad (49)$$

which is proportional to approximate $x_0(t)$ given in Eq. (38).